

# Single-pulse stimulated Raman scattering spectroscopy

Hadas Frostig,\* Ori Katz, Adi Natan, and Yaron Silberberg

Department of Physics of Complex Systems, The Weizmann Institute of Science, Rehovot 76100, Israel

\*Corresponding author: hadas.frostig@weizmann.ac.il

Received December 6, 2010; accepted February 16, 2011;

posted March 7, 2011 (Doc. ID 138876); published March 30, 2011

We demonstrate the acquisition of stimulated Raman scattering spectra with the use of a single femtosecond pulse. High-resolution vibrational spectra are obtained by shifting the phase of a narrow band of frequencies within the input pulse spectrum, using spectral shaping. The vibrational lines are resolved via amplitude features formed in the spectrum after interaction with the sample. Using this technique, low-frequency Raman lines ( $<100\text{ cm}^{-1}$ ) are observed on both the Stokes and anti-Stokes sides. © 2011 Optical Society of America

OCIS codes: 190.5650, 300.6420, 320.0320.

Coherent Raman scattering (CRS) spectroscopies provide high-sensitivity detection based on vibrational energy levels as an intrinsic contrast mechanism [1]. Until recently the dominant CRS spectroscopy technique has been coherent anti-Stokes Raman scattering (CARS). In the past several years, a different CRS process, stimulated Raman scattering (SRS), has been proven suitable for high-sensitivity microscopy applications as well [2,3].

In the common CARS and SRS schemes, a picosecond pump beam with frequency  $\omega_p$  and a picosecond Stokes beam with frequency  $\omega_s$  are focused onto the sample. When the beat frequency  $\omega_p - \omega_s$  matches a molecular vibrational frequency,  $\omega_{\text{vib}}$ , vibrations are resonantly excited. Probing photons of initial frequency  $\omega_{\text{pr}}$  scattered by the excited molecules are blueshifted or redshifted by  $\omega_{\text{vib}}$ . This results in the creation of two spectral sidebands around  $\omega_{\text{pr}}$ , at  $\omega_{\text{pr}} \pm \omega_{\text{vib}}$ . The vibrational spectrum is resolved by scanning the frequency of  $\omega_p$  or  $\omega_s$  and observing the intensity of the spectral sidebands. In practice, since CARS and SRS are third-order nonlinear processes, the intensity of the generated sideband field is weak compared to the incoming laser intensity. The straightforward approach, taken in CARS, is to observe the generated field at a frequency different from the input frequencies,  $\omega_{\text{cars}} = 2\omega_p - \omega_s$  ( $\omega_{\text{pr}} = \omega_p$ ). This allows the input frequencies to be filtered out, so that the weak signal can be detected. The CARS approach has proven beneficial in spectroscopy, microscopy, and biological imaging [1]. A known limitation of CARS, however, is that it suffers from an intense nonresonant background, which distorts the spectra and limits detection sensitivity.

In contrast, the approach taken in SRS is to observe the generated electric field at a frequency that is equal to one of the input frequencies, such as  $\omega_p = \omega_s + (\omega_p - \omega_s)$  (blueshifted sideband of  $\omega_{\text{pr}} = \omega_s$ ). This process is described in Fig. 1(a). When doing so, one observes the interference of the input field with the resonant and nonresonant generated fields. The most significant terms of the interference are given by

$$I_{\text{total}} = |E_{\text{in}} + E_{\text{nr}} + E_r|^2 \\ \cong I_{\text{in}} + 2|E_{\text{in}}||E_{\text{nr}}| \cos \phi_{\text{nr}} + 2|E_{\text{in}}||E_r| \cos \phi_r, \quad (1)$$

where  $E_{\text{in}}$  is the input electric field,  $E_{\text{nr}}$  and  $E_r$  are the third-order nonresonant and resonant electric field responses, respectively, and  $\phi_{\text{nr}}$  and  $\phi_r$  are their phases

with respect to  $E_{\text{in}}$ . The approximation in Eq. (1) is valid in the conventional scheme, where  $|E_{\text{in}}| \gg |E_r|, |E_{\text{nr}}|$ . The benefit of interference with the input field is twofold. First, as  $E_{\text{in}}$  and  $E_{\text{nr}}$  are in quadrature, the corresponding interference term vanishes ( $\cos \phi_{\text{nr}} = 0$ ). Second,  $E_{\text{in}}$  and  $E_r$ , which are not in quadrature, coherently interfere. This results in heterodyne amplification of  $E_r$ , much like in heterodyne CARS schemes [4]. The large background due to the input field [first term in Eq. (1)] is avoided by modulating either the pump or Stokes beams and measuring the output spectrum using lock-in detection [2]. Thus, the signal detected in practice corresponds to the third term in Eq. (1). Because of the line shape of the molecular resonance,  $E_r$  is phase-shifted from  $E_{\text{in}}$  such that the interference causes gain in the redshifted sideband ( $\cos \phi_r > 0$  for  $E_r(\omega_s)$ ) and loss in the blueshifted sideband ( $\cos \phi_r < 0$  for  $E_r(\omega_p)$ ). In accordance with theoretical analysis, previous SRS work has shown to provide high-sensitivity and display negligible nonresonant background, enabling the successful performance both in picosecond [2,3] and multiplex schemes [5]. However, these schemes make use of multibeam configurations and require maintaining spatial and temporal overlap of the beams on the sample. Development of a simpler SRS spectroscopy scheme can facilitate the integration of SRS into practical biomedical use.

Here we propose an SRS scheme in which full spectral information can be retrieved with the use of a single femtosecond pulse. In analogy to single-pulse CARS schemes [6,7], the use of a spectrally broad pulse provides both the pump and Stokes frequencies necessary for excitation and probing of a vibrational mode. The excitation is caused by all the frequency pairs with differences that match the vibrational frequency of the molecule. In the transform-limited case, the Raman level is probed by the entire pulse spectrum uniformly, which generates a spectrally broad gain-loss pattern as shown in Fig. 1(b) [8]. The overall interaction results in a small redshift of the pulse spectrum, without a clear molecular fingerprint. One possible method of regaining chemical specificity is to define a spectrally narrow probe in the broadband pulse spectrum using spectral shaping. This is accomplished by inducing a  $\pi$  phase shift in a narrow band of frequencies as shown in Fig. 1(c) (this phase pattern will be referred to as  $\pi$  phase gate). Since the shaping affects an insignificant portion of the input pulse, the excitation of the vibrational level is hardly modified. Thus,

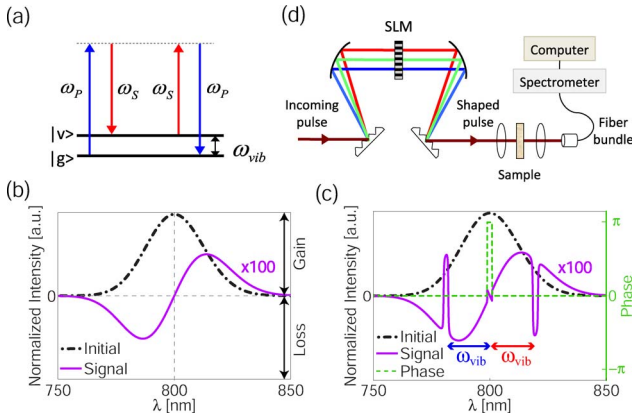


Fig. 1. (Color online) (a) Energy level diagram of the SRS process that creates signal at  $\omega_p$ . (b) Level spectra of the input pulse (black) and the resonant signal (purple) it generates from a sample with a single line at  $300\text{ cm}^{-1}$ . (c) Simulated spectrum (black) and phase (green) of a pulse shaped with a  $\pi$  phase gate and the spectrum of the resonant signal (purple) it generates from the same sample. The incoming pulses are phase-shaped using a liquid-crystal SLM. The beam is then focused onto the sample using a 15 cm lens and the transmitted light is collected by a 0.5 NA lens and coupled into a CCD-based spectrometer. For samples in powder form, the backscattered light is collected and coupled into the spectrometer.

the shaped spectrum can be thought of as the sum of a broadband excitation pulse and a narrowband probe pulse, similar to multiplex SRS schemes [5]. The interaction with the sample creates two sidebands of the probe pulse that are shifted by  $\pm\omega_{\text{vib}}$  from the phase gate frequency (purple curve in Fig. 1(c)). As a result of the  $\pi$  phase shift of the probe field, the  $E_r$  generated is  $\pi$  phase-shifted from the  $E_r$  of the picosecond scheme described above. Consequently the redshifted (Stokes) sideband causes loss ( $\cos\phi_r < 0$ ) and the blueshifted (anti-Stokes) sideband causes gain ( $\cos\phi_r > 0$ ). The sidebands induce distinct, spectrally narrow features in the broad gain–loss pattern caused by the excitation pulse, and the Raman lines can be easily read off.

To demonstrate single-pulse SRS (SPSRS) spectroscopy, we measured the vibrational spectra of several samples. The setup consisted of an amplified Ti:sapphire laser emitting  $\sim 30$  fs pulses centered at 795 nm ( $\sim 50$  nm bandwidth), a programmable pulse-shaper based on a spatial-light modulator (SLM) and a spectrometer [Fig. 1(d)]. The pulses were of varying energies in the range  $100\text{ nJ}$ – $1\text{ }\mu\text{J}$  at a 1 kHz repetition rate. In order to eliminate the input pulse background [first term in Eq. (1)], which is several orders of magnitude larger than the resonant signal, we conducted a differential measurement. The measurement was performed by comparing the spectra of the light exiting the sample for two slightly different spectral locations of the  $\pi$  phase gate. When subtracting the two, not only does the input pulse background vanish but also the broad gain–loss pattern caused by the excitation pulse [see Fig. 1(c)]. Therefore, on the anti-Stokes side for example, each Raman line is manifested as a narrow peak (probe sideband) and dip (subtracted peak) spectral feature on a rather flat background.

High-resolution Raman spectra of several materials are presented in Fig. 2. The measured spectra are in good agreement with the known vibrational spectra of these materials. The Raman lines can be easily identified either on the Stokes or the anti-Stokes side, allowing for flexibility in the experimental setup. We note that some of the resonant features slightly deviate from the expected peak–dip shape. This is the result of self-phase modulation (SPM) acquired through propagation in the sample, due to the large confocal parameters and thick samples (1 cm) we used. Using weaker input pulses (1–10 nJ) significantly reduces SPM and the expected peak–dip shape of the features is recovered. Nevertheless, even with propagation effects clear spectral features are visible, enabling spectroscopic identification. The demonstrated resolution is  $\sim 20\text{ cm}^{-1}$ , limited by the resolution of the SLM, which dictates the minimal phase gate width. Because of the simplicity of the measurement scheme, there is no need to filter out the excitation light. This is in contrast to many other filter-based Raman spectroscopy methods, in which the transition width of the filter is what limits the smallest Raman shift that can be measured. Consequently, low-frequency vibrational lines can be measured in a straightforward manner. As seen in Fig. 2(d), several low lines of sulfur at 217, 152, and  $83\text{ cm}^{-1}$  are easily discerned and a feature indicating the  $51\text{ cm}^{-1}$  is noticeable on the anti-Stokes side, all in agreement with previous work [9]. Generally, the lowest line that can be detected using this scheme is limited by the spectral width of the  $\pi$  phase gate. However, in thick samples, propagation effects in combination with the non-linear phase that is accumulated at high intensities can cause spectral changes in the vicinity of the  $\pi$  phase gate [10]. These changes impose a higher bound on the lowest detectable line, as in Fig. 2(d).

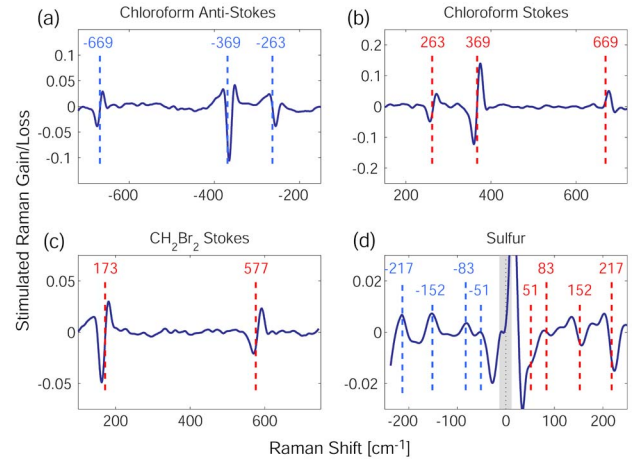


Fig. 2. (Color online) SPSRS spectra of several samples. The Raman lines are plotted on top for reference. (a) Chloroform anti-Stokes spectrum. (b) Chloroform Stokes spectrum. (c) Dibromomethane Stokes spectrum. (d) Powdered sulfur spectrum; the phase gate area is marked in gray. Spectra (a)–(c) were resolved from the difference between two measurements with a 400 ms integration time. Spectrum (d) was averaged over ten such differential measurements. The differences between the resonant feature shapes in (a) and (b), as well as the spectral features in the vicinity of the gate in (d), are due to propagation effects. These effects are substantially reduced when using weaker input pulses.

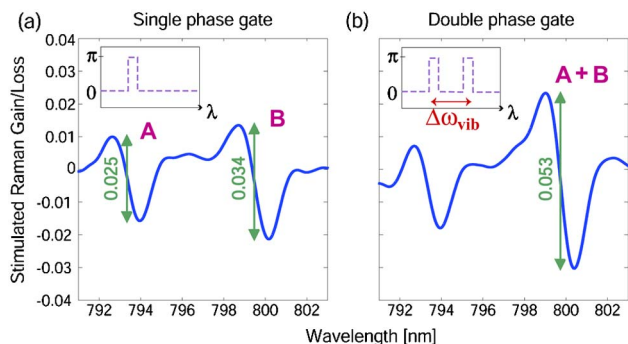


Fig. 3. (Color online) Coherent addition of Raman lines in carbon tetrachloride. (a) Spectrum generated by a pulse shaped with a single phase gate at 780 nm, showing two Raman lines:  $218\text{ cm}^{-1}$  (at 793 nm) and  $314\text{ cm}^{-1}$  (at 799 nm). (b) Spectrum generated by a pulse shaped with two phase gates at 780 and 786 nm. The  $314\text{ cm}^{-1}$  line of the first phase gate and the  $218\text{ cm}^{-1}$  line of the second phase gate both occur at 799 nm. The resulting peak-to-dip difference approximately equals the sum of the peak-to-dip differences of the two Raman lines in (a). Inset, corresponding spectral phase masks.

Another advantageous feature of SPSRS over other SRS schemes arises when the desired goal is detection of a predetermined substance. When applying several  $\pi$  phase gates to the spectrum spaced by the differences between the vibrational frequencies of the molecule, the peak-dip features from all the gates are generated at the same frequency. Because of the coherent nature of the process, the signals coherently combine to create a single larger spectral feature. This feature indicates the level of correlation between the measured spectrum and the known spectrum of a substance [11]. The benefits are enhanced signal-to-noise ratio (SNR) compared to each single line, as well as elimination of the need for postprocessing of the spectrum. The ability to coherently add lines using SPSRS is demonstrated in the spectrum of carbon tetrachloride, as shown in Fig. 3. The single-gate spectrum in Fig. 3(a) reveals two resonant lines, which create features at 793 and 799 nm. In the double-gated spectrum shown in Fig. 3(b) the two features are combined at 799 nm. The combined feature has a peak-to-dip difference that nearly equals (90%) the sum of the two individual lines, representing an appreciable enhancement of the SNR. The feature can be further enlarged by optimizing the relative phase of the gates and their spectral locations through the use of an adaptive algorithm [11].

In conclusion, we have demonstrated vibrational spectra acquisition using a single-pulse SRS scheme. Spectral shaping enables control over the interference of the input

field and the generated resonant electric field, facilitating the creation of narrow spectral features that indicate the vibrational frequencies. Using this method, all Raman lines within the detection range can be simultaneously identified in a similar fashion to multiplex SRS schemes but with a single beam setup. Two unique features of the SPSRS scheme have been demonstrated, the ability to distinguish low-lying Raman lines and the ability to coherently add the signal from several lines for an improved spectroscopic fingerprint. Spectroscopy of low-lying Raman lines is a useful tool in various research fields. Examples include monitoring electrically distinct carbon nanotubes [12], as well as studying the hydration dynamics of DNA films [13]. Furthermore, by employing fast shaping techniques together with lock-in detection [14] the sensitivity of our setup can be substantially increased and SPSRS may become an attractive scheme for microscopy and biological imaging.

The authors thank the Ministry of Science and Technology (MOST), the North Atlantic Treaty Organization (NATO), and the Crown Photonic Center for financial support.

## References

1. A. Volkmer, *J. Phys. D* **38**, R59 (2005).
2. C. W. Freudiger, W. Min, B. G. Saar, S. Lu, G. R. Holtom, C. He, J. C. Tsai, J. X. Kang, and X. S. Xie, *Science* **322**, 1857 (2008).
3. P. Nandakumar, A. Kovalev, and A. Volkmer, *New J. Phys.* **11**, 033026 (2009).
4. B. V. Vacano, T. Buckup, and M. Motzkus, *Opt. Lett.* **31**, 2495 (2006).
5. E. Ploetz, B. Marx, T. Klein, R. Huber, and P. Gilch, *Opt. Express* **17**, 18612 (2009).
6. D. Oron, N. Dudovich, and Y. Silberberg, *Phys. Rev. Lett.* **89**, 273001 (2002).
7. O. Katz, A. Natan, Y. Silberberg, and S. Rosenwaks, *Appl. Phys. Lett.* **92**, 171116 (2008).
8. N. Dudovich, D. Oron, and Y. Silberberg, *J. Chem. Phys.* **118**, 9208 (2003).
9. C. Moser and F. Havermeier, in *The Proceedings of 22nd International Conference on Raman Spectroscopy* (Academic, 2010), pp. 794–795.
10. D. R. Austin, J. A. Bolger, C. M. de Sterke, and B. J. Eggleton, *Opt. Express* **14**, 13142 (2006).
11. D. Oron, N. Dudovich, and Y. Silberberg, *Phys. Rev. A* **70**, 023415 (2004).
12. M. S. Strano, C. A. Dyke, M. L. Usrey, P. W. Barone, M. J. Allen, H. Shan, C. Kittrell, R. H. Hauge, J. M. Tour, and R. E. Smalley, *Science* **301**, 1519 (2003).
13. H. Urabe, Y. Sugawara, M. Ataka, and A. Rupperecht, *Biophys. J.* **74**, 1533 (1998).
14. E. Frumker and Y. Silberberg, *Opt. Lett.* **32**, 1384 (2007).